EUROPEAN ORGANIZATION FOR NUCLEAR RESEARCH

Proposal to the ISOLDE and Neutron Time-of-Flight Committee

Collinear resonance ionization spectroscopy of neutron-deficient antimony isotopes, towards the proton drip line

January 11, 2023

K. M. Lynch[1], M. Athanasakis-Kaklamanakis[2,3], S. W. Bai[4], Y. Balasmeh[2], T. E. Cocolios[2], R. P. de Groote[2], C. Fajardo[2], K. T. Flanagan[1,5], S. Franchoo[6], R. F. Garcia Ruiz[7], S. Geldhof[8], G. Georgiev[6], D. Hanstorp[9], R. Heinke[10], A. Koszorús[2,11], L. Lalanne[3], Y. C. Liu[4], Y. S. Liu[4], A. McGlone[1], G. Neyens[2], M. Nichols[9], F. Pastrana[7], H. Perrett[1], J. R. Reilly[1], J. Trujillo[2], B. van den Borne[2], J. Wessolek[1], S. G. Wilkins[7] and X. F. Yang[4].

[1]*School of Physics and Astronomy, The University of Manchester, Manchester M13 9PL, UK*
[2]*KU Leuven, Instituut voor Kern- en Stralingsfysica, B-3001 Leuven, Belgium*
[3]*Experimental Physics Department, CERN, CH-1211 Geneva 23, Switzerland*
[4]*School of Physics and State Key Laboratory of Nuclear Physics and Technology, Peking University, Beijing 100971, China*
[5]*Photon Science Institute, The University of Manchester, Manchester M13 9PY, UK*
[6]*IJCLab, Université Paris-Saclay, CNRS/IN2P3, IJCLab, 91405 Orsay, France*
[7]*Department of Physics, Massachusetts Institute of Technology, Cambridge, MA 02139, USA*
[8]*GANIL, CEA/DRF-CNRS/IN2P3, B.P. 55027, 14076 Caen, France*
[9]*Department of Physics, University of Gothenburg, SE 412 96 Gothenburg, Sweden*
[10]*Accelerator Systems Department, CERN, CH-1211 Geneva 23, Switzerland*
[11]*Belgian Nuclear Research Centre (SCK•CEN), Boeretang 200, 2400, Mol, Belgium*

Spokesperson: Kara Marie Lynch [kara.lynch@manchester.ac.uk]
Contact person: Louis Lalanne [louis-alexandre.lalanne@cern.ch]

CERN-INTC-2023-016 / INTC-P-657
11/01/2023

Abstract: We propose to study the hyperfine structure of the neutron-deficient Sb (Z=51) isotopes with the CRIS experiment, so that we may test our understanding of the effect of the valence proton on the nuclear structure around the Z=50 shell closure. From hyperfine structure measurements, the nuclear spins, electromagnetic moments and changes in mean square charge radii can be determined and compared to theoretical predictions from density functional theory and *ab-initio* calculations. As we move towards the proton drip line at ^{105}Sb (N=54), we will also be able to investigate the

effects of the unbound proton on the nuclear properties. With a single proton outside the Z=50 shell closure, the antimony isotopes represent a simple and rigorous test for our nuclear theories, providing important information to benchmark them.

Requested shifts: 19 shifts with protons (+3 shifts without protons for setup)

1 Introduction

Doubly-magic nuclei represent cornerstones in our understanding of the nuclear many-body problem. Recent advances in both *ab-initio* nuclear theory and computational power have forged the way to provide theoretical descriptions of increasingly more complex nuclei, now reaching as far as the doubly-magic ^{100}Sn (Z, N=50) and ^{132}Sn (Z=50, N=82) nuclei [1, 2]. Motivated by the chance to test these descriptions, and benchmark the nuclear properties to aid advancement, there has been an enthusiastic experimental effort in recent years to understand the evolution of nuclear properties around the closed proton shell Z=50, between the closed neutron shells N=50 and N=82. This region of the nuclear chart has seen comprehensive laser spectroscopy studies being performed on the nearby silver (Z=47) isotopes [3, 4], cadmium (Z=48) isotopes [5, 6], the neutron-deficient [7] and neutron-rich [8, 9] indium (Z=49) isotopes, the neutron-deficient [10] and neutron-rich [11, 12, 13] tin (Z=50) isotopes and the neutron-rich antimony (Z=51) isotopes [14]. In addition, experiments are planned for the neutron-rich tellurium (Z=52) isotopes [15].

2 Physics Motivation

As the heaviest self-conjugate doubly-magic nucleus, ^{100}Sn represents a unique laboratory with which to test our understanding of the nuclear many-body problem. By extension, the nuclei in the vicinity of ^{100}Sn allow us to evaluate our theoretical descriptions of their nuclear properties and behaviour. With one valence proton outside the closed Sn (Z=50) shell core, studying the antimony isotopes with laser spectroscopy provides the opportunity to examine and improve our understanding of the nuclear structure and the single-particle behaviour predicted by the spherical shell model, see Figure 1. This proposal follows a dedicated effort by the CRIS collaboration to understand nuclei

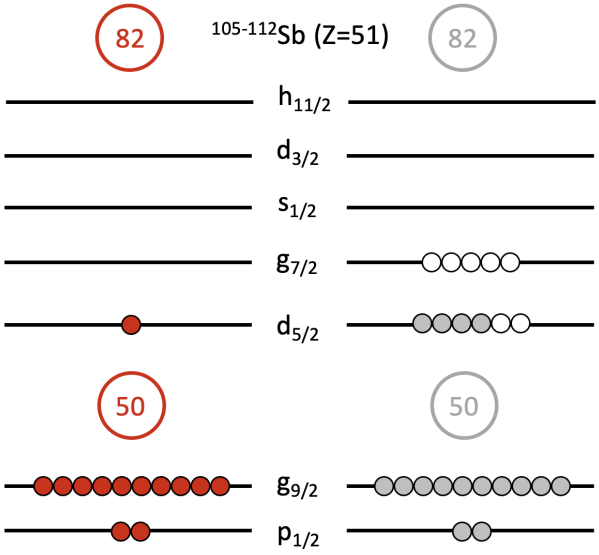

Figure 1: Occupation of nuclear orbitals for protons (red) and neutrons (grey) for the neutron-deficient Sb (Z=51) isotopes, from ^{105}Sb (N=54) (closed markers) to ^{112}Sb (N=61) (open markers).

in this region, having recently studied the neutron-deficient silver (Z=47) [16], indium (Z=49) [17] and tin (Z=50) [10, 18] isotopes.

2.1 Neutron-deficient antimony

In the shell model picture, the ground states of the neutron-deficient odd-A antimony isotopes are dominated by the valence proton in the $d_{5/2}$ nuclear orbital, as evidenced by the $5/2^+$ ground state spins for $^{\leq 121}$Sb. This can be seen in Figure 2(top) where the ground-state spin changes from $7/2^+$ to $5/2^+$ at ^{123}Sb (N=71) due to the re-ordering of the $d_{5/2}$ and $g_{7/2}$ proton orbitals (above the Z=50 core, see Figure 1) caused by the mass-dependent spin-orbit interaction. As we go more neutron deficient, depleting the neutron $g_{7/2}$ and $d_{5/2}$ orbitals, the persistence of the $5/2^+$ ground state will be investigated and the nuclear spins determined. Figure 2 presents the g-factors ($g = \mu_N/I$) for the previously-measured antimony isotopes, with the shaded area illustrating the neutron-deficient isotopes proposed to be studied. While not included in Figure 2 for clarity, the antimony isotopes also display rich isomerism - both short-lived (∼ns) and longer-lived (>ms) states exist. Measurement of both the ground state and any longer-lived isomeric states allow the evolution of both single-particle and collective behaviour to be investigated as the proton-to-neutron ratio equalises.

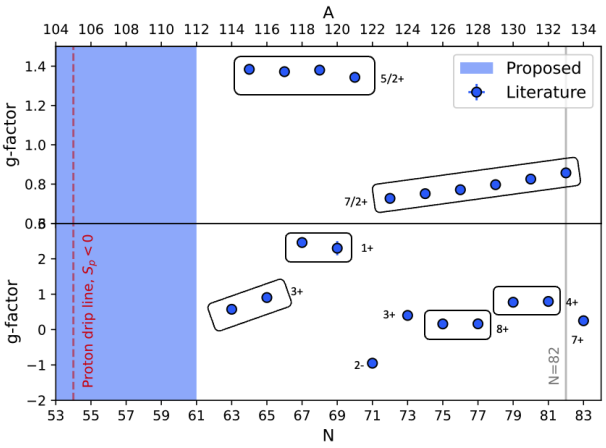

Figure 2: g-factors ($g = \mu_N/I$) for the previously-measured (top) odd-A and (bottom) odd-odd Sb isotopes (data markers) between the N=50 and N=82 shell closures [19, 14]. The blue shaded area illustrates the neutron-deficient Sb isotopes proposed to be studied.

With the existence of low-lying isomers and relatively large B(E2) values (known down to ^{104}Sn) suggesting a somewhat collective picture of the neutron-deficient Sn isotopes, recent Monte Carlo shell model calculations for the $^{100-132}$Sn isotopes have explained the increase in B(E2) values around ^{110}Sn as a consequence of shape evolution driven by proton excitations from the $1g_{9/2}$ orbital [1]. Suggesting a breaking of the Z=50 magic core, the authors expressed an urgent interest in the charge radii of neighbouring nuclei. The recent charge radii measurements of ^{104}Sn and ^{106}Sn isotopes, however, suggest a rapid reduction of collectivity towards the doubly magic ^{100}Sn [18]. *Ab-initio* calculations, while struggling to reproduce the absolute magnitude of the charge radii (a known challenge), provide a good description of the relative changes in the charge radii – even reproducing the suggested sub-shell closure at N=64 [10]. Further evidence for the doubly-magic nature of ^{100}Sn is provided by the existence of the largest-ever Gamow-Teller strength for the beta-decay of ^{100}Sn [20], as well as the large 'kink' in the charge radii of the neutron-deficient Ag (Z=47) isotopes as the N=50 shell is crossed [4]. Complementary evidence for the doubly-magic nature of ^{100}Sn has also been found when investigating the charge radii and quadrupole moments of the

neutron-deficient In (Z=49) isotopes [17]. As with the Sn isotopes, the In isotopes display a reduction in quadrupole moments and differential charge radii towards N=50, which is closely reproduced by predictions from density functional theory [9]. As the valence-proton analogue to indium, studying the antimony isotopes will test the robustness of the closed Sn core from above the shell closure and investigate the symmetry between the proton-hole and proton-particle approach.

2.2 Towards the proton drip line

The ultimate goal of this experimental campaign is to measure across the proton drip line at ^{105}Sb, where S_p becomes negative, in order to simultaneously investigate the role of the valence proton (above the Sn core) and the role of the unbound proton (as we cross the proton drip line). Measurement of the charge radii of nuclei beyond the proton drip line offers an exciting opportunity to measure the change in deformation that occurs when the protons are no longer bound in the nucleus by the strong force. This proposal seeks to explore the possibility of studying the 'proton-emitting' ^{105}Sb with the Decay Spectroscopy Station (DSS) at CRIS. The existence of ^{105}Sb as a proton emitter is contested in the literature – observation of a 1% branching ratio of proton emission (with an energy of 478(15) keV) at Berkeley in 1994 [21] has yet to be confirmed in subsequent experiments at GSI [22, 23]. While both the Berkeley and GSI experiments produced ^{105}Sb by fusion-evaporation reactions induced by a ^{58}Ni beam on a ^{50}Cr target, the Berkeley experiment transferred the ^{105}Sb isotopes to a counting station via a helium jet which took ∼25 ms. At GSI, the ^{105}Sb isotopes were collected on a transport tape and moved to the counting position every 2.8 s, and hence began counting after a longer time-period had elapsed than in the Berkeley experiment. One explanation that proton emission was only observed at Berkeley could be that there is a *short-lived* (ground or isomeric) state of ^{105}Sb that decays via proton emission. Measurements of the short-lived ^{214}Fr, with a half-life of 5.0(2) ms, have already been achieved at CRIS [24], as well as measurements of the low-yield ^{78}Cu isotope with a production rate of 20 ions/s [25]. With improvements to our sensitivity and selectivity already underway (e.g. field-ionization schemes, see below), yields measurements of ^{106}Sn and ^{105}Sb will allow us to assess the feasibility of laser spectroscopy measurements. By the identification of extra peaks in a hyperfine structure, the presence of an isomeric state is easily identifiable with laser spectroscopy. Furthermore, with the ability of CRIS to selectively ionize only the ground- or isomeric state, each nuclear state can be individually deflected to the DSS for proton-decay measurements – providing the opportunity to solve this proton-emission puzzle.

2.3 Nuclear theory

Results will be compared to state-of-the art nuclear theory. Density functional theory (DFT) can describe bulk properties of the nucleus (such as charge radii and binding energy) across the nuclear chart [26]. Calculations using the Gamow Coupled Channel approach and time-dependent DFT will provide precise predictions about the nuclear charge distribution and its electromagnetic moments [27, 28]. Furthermore, as we study the isotopes towards the proton drip line, we will be able to investigate the

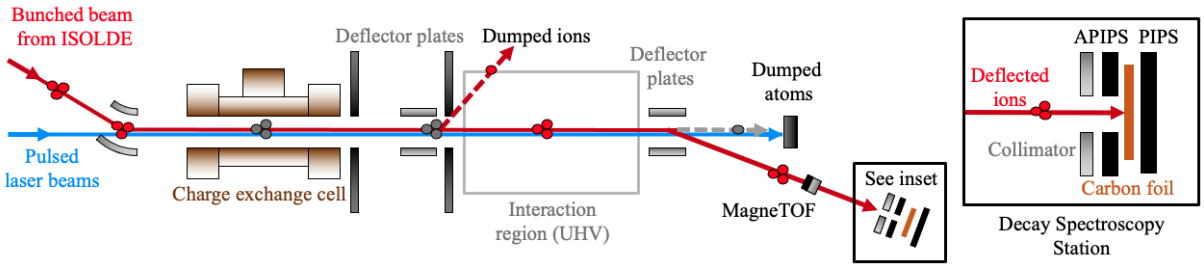

Figure 3: Schematic of the CRIS experiment. Laser-ionized ions can be deflected to a MagneTOF for hyperfine-structure measurements or the Decay Spectroscopy Station (inset) for proton-decay measurements. Figure modified from [32].

coupling between bound and unbound nuclear states, and the proton continuum [29]. By using different energy density functionals, the influence of different variations (e.g. relativistic/spin-orbit corrections, time-odd components etc.) on the charge radii can be investigated [30]. For example, the inclusion of surface and pairing terms has been crucial for reproducing the charge radii of the Ca isotopes [31], while the inclusion of time-odd terms were essential for reproducing the magnetic moments of the In isotopes [8].

Ab-initio valence-space in-medium similarity renormalization group (VS-IMSRG) calculations will also provide insights into the charge radii of the Sb isotopes – the interplay between the bulk properties (given by nuclear saturation density) and the local features (reflecting structural changes). While VS-IMSRG calculations struggle to reproduce the magnitude of the (absolute) charge radii, they have seen to be crucial in understanding the microscopic structure of the odd-even staggering (OES) of the charge radii of the Cu isotopes [25]. The OES, highly dependent on the nuclear shell structure and many-body correlations, offer the opportunity to test the orbital components of the nuclear wave function, benchmarking the theory as we measure towards the proton drip line.

3 Experimental Method

The antimony isotope of interest is laser-ionized with RILIS [33], mass-selected with HRS, bunched with ISCOOL and deflected into the CRIS beamline, see Figure 3. The antimony ions are neutralised by passing them through a potassium-vapour charge-exchange cell and the non-neutralised component of the beam is deflected away. Potassium is chosen over sodium for charge exchange due to the increased population of antimony produced in its atomic ground state during the neutralisation process. At a beam energy of 40 keV, it is predicted that 22% of the atomic population of antimony will be in the ground state ($5s^25p^3\ {}^4S_{3/2}$) when neutralised with potassium, compared to 19% with

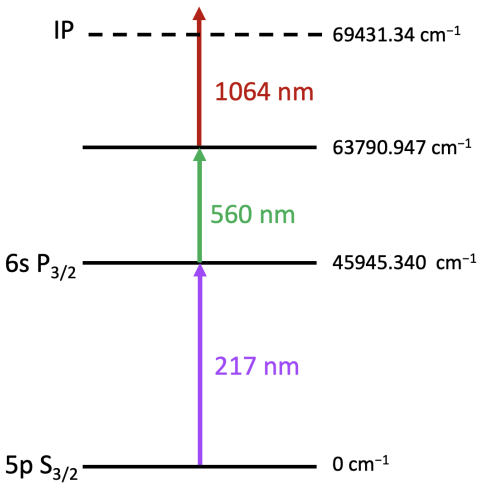

Figure 4: Resonance ionization scheme. The 217-nm resonant excitation step was used in previous work [14].

sodium [34]. The neutralised atoms pass into the interaction region, held at ultra-high vacuum, and are temporally and collinearly overlapped with three co-propagating pulsed laser beams to step-wise excite and ionize the isotope of interest.

The resonance ionization scheme for the antimony isotopes is shown in Figure 4. The hyperfine structure of the $5s^25p^3\ ^4S_{3/2} \rightarrow 5s^25p^2\ 6s\ ^4P_{3/2}$ atomic transition will be probed, by scanning the frequency of the 217-nm resonant-excitation laser light. The 217-nm laser light will be produced by frequency quadrupling 870-nm laser light from a narrow-band injection-seeded Ti:Sa laser. The 560-nm laser light for the second step will be produced from a Spectron Spectrolase 4000 pulsed dye laser (PDL) using Rhodamin 6G laser dye. The final non-resonant 1064-nm laser light will be produced from a Litron TRLi Nd:YAG laser. The laser-ionized ions are then deflected through 34-degrees and detected by a ETP MagneTOF particle detector or implanted into the DSS for decay measurements (or decay tagging). Scanning the frequency of the first resonant-excitation step probes the hyperfine structure of the isotope under investigation. From the atomic hyperfine structure, determination of the nuclear observables (spin, magnetic moment, quadrupole moment and isotope shift) is achieved without introducing any assumptions associated with a particular nuclear model.

3.1 Experimental considerations

All laser systems are currently available at CRIS. Significant investment has been made at CRIS in recent years to create a suite of laser systems that offers flexibility and redundancies. To that end, there are multiple laser systems available that can produce the necessary laser frequencies, thus avoiding a single laser failure resulting in a cancelled experiment. Soon to be added is a high-energy broadly tunable DPSS laser, integrating a diode pumped Nd:YAG laser and Optical Parameteric Oscillator (OPO) which will allow frequency scanning from 405 nm to 2600 nm. This OPO laser will also be able to provide 560-nm laser light for the second step in the laser scheme, should the need arise.

It is envisaged that initial measurements of the neutron-deficient isotopes will use an intermediate-band 217-nm laser light from a grating Ti:Sa, with a linewidth of $\sim$3 GHz, allowing measurement of the magnetic moments and isotopes shifts. As evidenced by recent measurements [14], the hyperfine structure of the antimony isotopes is relatively large (i.e. $\sim$5-10 GHz). Using a laser with a lower-resolution linewidth will aid the search for a resonant signal for the lower-yield isotopes. Once the resonant signal has been located, the hyperfine structure will be scanned using the narrow-band injection-seeded Ti:Sa laser (mentioned above), with a linewidth of $\sim$100 MHz. The synergistic approach of (1) searches with intermediate-band light and (2) measurements with narrow-band light will reduce our measurement time for each isotope.

In order to maximise the signal-to-noise ratio so that we may study these low-yield isotopes, minimisation of the background ions is essential. These background ions may be due to collisions with residual gas in the interaction region (i.e. collisional ions), non-resonant laser ionization of species in the atomic bunch or field-ionization of high-lying

Isotope	Half-life	Predicted yield (ions/s)	Shifts requested	New results
^{123}Sb	Stable	3.0×10^{6}	3 (without protons)	-
$^{112-121}$Sb	>53.5 s	$>7.0\times10^{5}$	5	-
^{111}Sb	75 s	5.1×10^{5}	0.5	μ, Q_s, $\delta\langle r^2\rangle$
^{110}Sb	23 s	2.7×10^{4}	1	I, μ, Q_s, $\delta\langle r^2\rangle$
^{109}Sb	17 s	4.1×10^{3}	2	μ, Q_s, $\delta\langle r^2\rangle$
^{108}Sb	7.4 s	1.9×10^{2}	4	μ, Q_s, $\delta\langle r^2\rangle$
^{107}Sb	4.0 s	1.7×10^{1}	6	μ, Q_s, $\delta\langle r^2\rangle$
^{106,105}Sb	0.6 s, 1.22 s	1.3×10^{-1}	0.5	μ, Q_s, $\delta\langle r^2\rangle$

Table 1: Isotopes of interest, half-lives, predicted yields from a LaC target, number of shifts requested and potential new results. 3 shifts (without protons) are requested before the experiment for beam tuning, charge-exchange cell heating and laser/atom interaction optimization. 0.5 shifts are requested after the experiment for yield/background measurements of ^{105}Sb to guide future proposals.

states in the strong electric-field region around the 34-degree bend (that deflect ions to the MagneTOF detector) [17]. Collisional ionization is minimized by the ultra-high vacuum conditions of the interaction region, now routinely in the 10^{-10} mbar range. In the mass range of the neutron-deficient antimony isotopes, the main source of background is expected to be indium and stable molecules (e.g. SrF^{+}). Previous CRIS experiments on the indium isotopes observed resonant structures (e.g. in ^{101}In) that were due to excitations of transitions in stable molecules in the ion beam, that were close in frequency to the indium excitation transitions [17]. Using 1064-nm laser light as the final step, rather than the higher-energy 532-nm laser light, will reduce non-resonant ionization of stable molecules. An additional option is to replace the final non-resonant laser step with a field-ionization scheme. In such a scheme, the antimony isotopes are excited into a (known) Rydberg state [35] and ionized in a high-electric field region (i.e. the field-ionization unit). By separating ions created before the unit from the neutral atoms, all laser-related background effects can be removed, as well as reducing the collisional background (by a factor of 100) [17]. A proof-of-principle apparatus has already been demonstrated [36] and an improved design is soon to be installed in the CRIS beam line. It is to be noted that while background species will be present during our studies of the neutron-deficient antimony isotopes, the proposed experiment is feasible with the current CRIS experimental setup.

4 Beam Time Request

In total, we request **18.5** shifts with protons using a **LaC target** with **RILIS**. The requested shifts for each isotope include the time necessary to perform regular calibration measurements with ^{123}Sb. Scans of previously measured $^{112-123}$Sb isotopes [14] are needed for ISCOOL voltage calibrations and accurate extraction of isotope shifts. We request 3 shifts (without protons) before the experiment to perform beam tuning, charge-exchange cell heating and laser/atom interaction optimization. We also request 0.5 shifts after the experiment for yield and background measurements of ^{106,105}Sb. These measurements are necessary to gauge the possibility of studying the antimony isotopes at the proton drip line, and to guide developments that may be required for future proposals/addendum.

A summary of the predicted yields and requested shifts are presented in Table 4. As only historic yield measurements from the SC are available, yields have been predicted using FLUKA calculations and an experimentally-determined release fraction – please see Appendix [37]. For all isotopes with a yield above 10^5 ions/s, measurement times will not be limited by yield or statistics, but by the time taken to scan the laser frequency and perform regular reference measurements. We therefore count 0.5 shifts per isotope, due to the large hyperfine splitting of antimony. For the lower-yield isotopes, shift estimates were based on previous experiences measuring isotopes with large hyperfine splitting (e.g. In [38], Ag [39], Cu [25]). For instance, for ^{78}Cu, produced at a rate of 20 ions/s, one shift was sufficient to scan a frequency range of 2 GHz [25]. For ^{107}Sb (with a predicted yield of 17 ions/s and a scan range of up to 6 GHz), 3 shifts would be required for a complete scan (and thus a total of 6 shifts for two complete scans).

Summary of requested shifts: 18.5 shifts for hyperfine structure measurements, 3 shifts (without protons) for setup and 0.5 shifts for yield/background measurements.

References

[1] T. Togashi, Y. Tsunoda, T. Otsuka, N. Shimizu, M. Honma, Phys. Rev. Lett. **121**, 062501 (2018)

[2] P. Arthuis, C. Barbieri, M. Vorabbi, P. Finelli, Phys. Rev. Lett. **125**, 182501 (2020)

[3] R. Ferrer, N. Bree, T. Cocolios, I. Darby, H. De Witte, W. Dexters, J. Diriken, J. Elseviers, S. Franchoo, M. Huyse et al., Physics Letters B **728**, 191 (2014)

[4] M. Reponen, R.P. de Groote, L. Al Ayoubi, O. Beliuskina, M.L. Bissell, P. Campbell, L. Cañete, B. Cheal, K. Chrysalidis, C. Delafosse et al., Nature Communications **12**, 4596 (2021)

[5] D.T. Yordanov, D.L. Balabanski, J. Bieroń, M.L. Bissell, K. Blaum, I. Budinčević, S. Fritzsche, N. Frömmgen, G. Georgiev, C. Geppert et al., Phys. Rev. Lett. **110**, 192501 (2013)

[6] M. Hammen, W. Nörtershäuser, D.L. Balabanski, M.L. Bissell, K. Blaum, I. Budinčević, B. Cheal, K.T. Flanagan, N. Frömmgen, G. Georgiev et al., Phys. Rev. Lett. **121**, 102501 (2018)

[7] R.F. Garcia Ruiz et al., Tech. rep., CERN-INTC-2017-055, INTC-P-504-ADD-1, https://cds.cern.ch/record/2266800 (2017)

[8] A.R. Vernon, R.F. Garcia Ruiz, T. Miyagi, C.L. Binnersley, J. Billowes, M.L. Bissell, J. Bonnard, T.E. Cocolios, J. Dobaczewski, G.J. Farooq-Smith et al., Nature **607**, 260 (2022)

[9] J. Karthein et al. (2023), in progress

[10] F. Gustafsson et al. (2023), in progress

[11] C. Gorges, L.V. Rodríguez, D.L. Balabanski, M.L. Bissell, K. Blaum, B. Cheal, R.F. Garcia Ruiz, G. Georgiev, W. Gins, H. Heylen et al., Phys. Rev. Lett. **122**, 192502 (2019)

[12] D.T. Yordanov, L.V. Rodríguez, D.L. Balabanski, J. Bieroń, M.L. Bissell, K. Blaum, B. Cheal, J. Ekman, G. Gaigalas, R.F. Garcia Ruiz et al., Communications Physics **3**, 107 (2020)

[13] L.V. Rodríguez, D.L. Balabanski, M.L. Bissell, K. Blaum, B. Cheal, G. De Gregorio, J. Ekman, R.F. Garcia Ruiz, A. Gargano, G. Georgiev et al., Phys. Rev. C **102**, 051301 (2020)

[14] S. Lechner, Z.Y. Xu, M.L. Bissell, K. Blaum, B. Cheal, G. De Gregorio, C.S. Devlin, R.F. Garcia Ruiz, A. Gargano, H. Heylen et al., Phys. Rev. C **104**, 014302 (2021)

[15] L.V. Rodridguez et al., Tech. rep., CERN-INTC-2020-036, INTCP-561, http://cds.cern.ch/record/2752999 (2020)

[16] R. de Groote et al., Tech. rep., CERN-INTC-2020-023, INTC-P-551, https://cds.cern.ch/record/2717869 (2020)

[17] C. Ricketts, Ph.D. thesis, The University of Manchester, https://cds.cern.ch/record/2799932 (2021)

[18] F.P. Gustafsson, Ph.D. thesis, KU Leuven, https://cds.cern.ch/record/2799928 (2021)

[19] N. Stone, Atomic Data and Nuclear Data Tables **90**, 75 (2005)

[20] C.B. Hinke, M. Böhmer, P. Boutachkov, T. Faestermann, H. Geissel, J. Gerl, R. Gernhäuser, M. Górska, A. Gottardo, H. Grawe et al., Nature **486**, 341 (2012)

[21] R.J. Tighe, D.M. Moltz, J.C. Batchelder, T.J. Ognibene, M.W. Rowe, J. Cerny, Phys. Rev. C **49**, R2871 (1994)

[22] M. Shibata, Z. Hu, J. Agramunt, D. Cano-Ott, R. Collatz, M. Górska, H. Grawe, M. Hellström, Z. Janas, M. Karny et al., Phys. Rev. C **55**, 1715 (1997)

[23] Z. Liu, P.J. Woods, K. Schmidt, H. Mahmud, P.S.L. Munro, A. Blazhev, J. Döring, H. Grawe, M. Hellström, R. Kirchner et al., Phys. Rev. C **72**, 047301 (2005)

[24] G.J. Farooq-Smith, T.E. Cocolios, J. Billowes, M.L. Bissell, I. Budinčević, T. Day Goodacre, R.P. de Groote, V.N. Fedosseev, K.T. Flanagan, S. Franchoo et al., Phys. Rev. C **94**, 054305 (2016)

[25] R.P. de Groote, J. Billowes, C.L. Binnersley, M.L. Bissell, T.E. Cocolios, T. Day Goodacre, G.J. Farooq-Smith, D.V. Fedorov, K.T. Flanagan, S. Franchoo et al., Nature Physics **16**, 620 (2020)

[26] P.G. Reinhard, W. Nazarewicz, Phys. Rev. C **103**, 054310 (2021)

[27] S.M. Wang, W. Nazarewicz, Phys. Rev. Lett. **120**, 212502 (2018)

[28] S.M. Wang, W. Nazarewicz, Phys. Rev. Lett. **126**, 142501 (2021)

[29] A.J. Miller, K. Minamisono, A. Klose, D. Garand, C. Kujawa, J.D. Lantis, Y. Liu, B. Maaß, P.F. Mantica, W. Nazarewicz et al., Nature Physics **15**, 432 (2019)

[30] J. Hur, D.P.L. Aude Craik, I. Counts, E. Knyazev, L. Caldwell, C. Leung, S. Pandey, J.C. Berengut, A. Geddes, W. Nazarewicz et al., Phys. Rev. Lett. **128**, 163201 (2022)

[31] P.G. Reinhard, W. Nazarewicz, Phys. Rev. C **95**, 064328 (2017)

[32] K.M. Lynch, J. Billowes, M.L. Bissell, I. Budinčević, T.E. Cocolios, R.P. De Groote, S. De Schepper, V.N. Fedosseev, K.T. Flanagan, S. Franchoo et al., Phys. Rev. X **4**, 011055 (2014)

[33] V.N. Fedosseev, B.A. Marsh, D.V. Fedorov, U. Köster, E. Tengborn, Hyperfine Interactions **162**, 15 (2005)

[34] A. Vernon, J. Billowes, C. Binnersley, M. Bissell, T. Cocolios, G. Farooq-Smith, K. Flanagan, R. Garcia Ruiz, W. Gins, R. de Groote et al., Spectrochimica Acta Part B: Atomic Spectroscopy **153**, 61 (2019)

[35] R. Li, J. Lassen, J. Ruczkowski, A. Teigelhöfer, P. Bricault, Spectrochimica Acta Part B: Atomic Spectroscopy **128**, 36 (2017)

[36] A.R. Vernon, C.M. Ricketts, J. Billowes, T.E. Cocolios, B.S. Cooper, K.T. Flanagan, R.F. Garcia Ruiz, F.P. Gustafsson, G. Neyens, H.A. Perrett et al., Scientific Reports **10**, 12306 (2020)

[37] S. Stegemann, *Private communication* (2022)

[38] S. Wilkins et al., Tech. rep., CERN-INTC-2022-048 ; INTC-P-646, https://cds.cern.ch/record/2834696 (2022)

[39] R. de Groote et al., Tech. rep., CERN-INTC-2020-023 ; INTC-P-551, https://cds.cern.ch/record/2717869 (2020)

DESCRIPTION OF THE PROPOSED EXPERIMENT
Please describe here below the main parts of your experimental set-up:

Part of the experiment	Design and manufacturing
CRIS experiment	☒ To be used without any modification

HAZARDS GENERATED BY THE EXPERIMENT
Hazards named in the document relevant for the fixed CRIS installation

APPENDIX

Yield Predictions

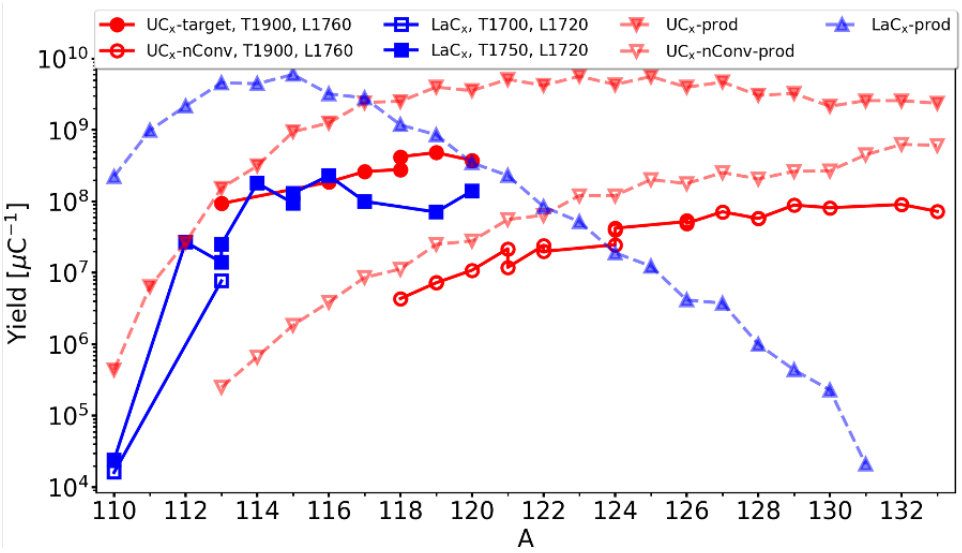

Figure 5: Overview of Sb production. Solid lines are experimentally measured yields. Dashed lines are FLUKA simulation in-target production yields. Figure kindly provided by S. Stegemann [37].

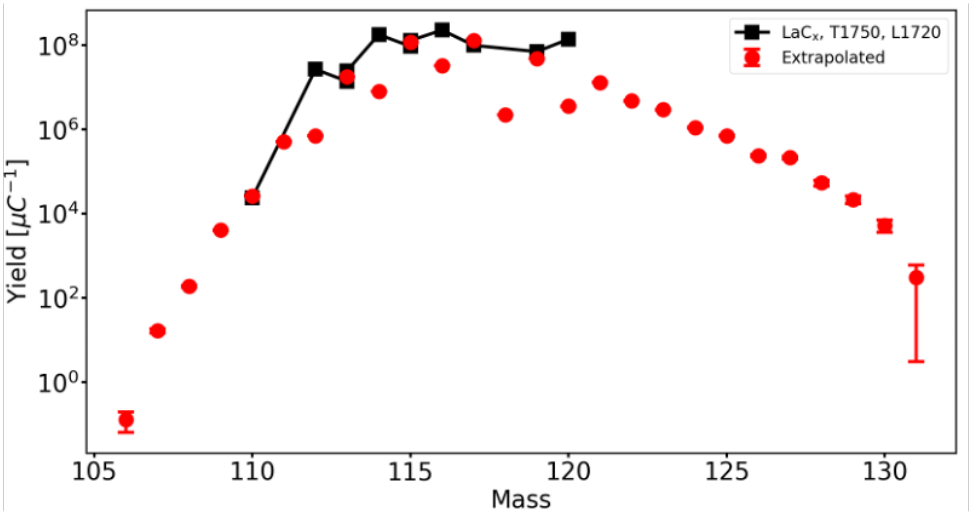

Figure 6: Predicted Sb yields based on extrapolation. Figure kindly provided by S. Stegemann [37].